The exponential decline in saturated hydraulic conductivity with depth: a novel method for exploring its effect on water flow paths and transit time distribution

A. A. Ameli,[1,2,3]* J. J. McDonnell[2,4] and K. Bishop[3,5]

[1] *Department of Biology, University of Western Ontario, Ontario, Canada*
[2] *Global Institute for Water Security, University of Saskatchewan, Saskatoon, Canada*
[3] *Department of Earth Sciences, Air Water and Landscape Sciences, Uppsala University, Uppsala, Sweden*
[4] *School of Geosciences, University of Aberdeen, Aberdeen, UK*
[5] *Department of Aquatic Sciences and Assessment, Swedish University of Agricultural Sciences, (SLU), Uppsala, Sweden*

Abstract:

The strong vertical gradient in soil and subsoil saturated hydraulic conductivity is characteristic feature of the hydrology of catchments. Despite the potential importance of these strong gradients, they have proven difficult to model using robust physically based schemes. This has hampered the testing of hypotheses about the implications of such vertical gradients for subsurface flow paths, residence times and transit time distribution. Here we present a general semi-analytical solution for the simulation of 2D steady-state saturated-unsaturated flow in hillslopes with saturated hydraulic conductivity that declines exponentially with depth. The grid-free solution satisfies mass balance exactly over the entire saturated and unsaturated zones. The new method provides continuous solutions for head, flow and velocity in both saturated and unsaturated zones without any interpolation process as is common in discrete numerical schemes. This solution efficiently generates flow pathlines and transit time distributions in hillslopes with the assumption of depth-varying saturated hydraulic conductivity. The model outputs reveal the pronounced effect that changing the strength of the exponential decline in saturated hydraulic conductivity has on the flow pathlines, residence time and transit time distribution. This new steady-state model may be useful to others for posing hypotheses about how different depth functions for hydraulic conductivity influence catchment hydrological response. Copyright © 2015 John Wiley & Sons, Ltd.

KEY WORDS   exponential decline in saturated hydraulic conductivity with depth; semi analytical model; integrated flow and transport model; transit time distribution; subsurface flow pathline; Saturated-Unsaturated flow

Received 29 September 2015; Accepted 15 December 2015

INTRODUCTION

The exponential decline in saturated hydraulic conductivity (K_s) with depth is a hallmark of hillslope and catchment hydrology. Classic studies (e.g. Weyman, 1973; Harr, 1977; Anderson and Burt, 1978) have shown this empirically, and such distributions are a ubiquitous feature of forest soils. The rapid decline in K_s with depth was a central feature of Keith Beven's TOPMODEL (Beven and Kirkby, 1979) that ushered a revolution in semi-distributed modelling approaches. TOPMODEL captures this key feature of soil structure by allowing lateral flow to increase exponentially as precipitation or snowmelt raise the water table closer and closer to the ground surface. In Scandinavia and other till mantled terrain, such processes have been studied extensively where the term 'transmissivity feedback' is now used to describe the phenomenological behaviour linked to the exponential K_s decline with depth (Lundin, 1982; Rodhe, 1989; Nyberg, 1995; Bishop *et al.*, 2004; Bishop *et al.*, 2011; Seibert *et al.*, 2011).

The exponential decline in K_s with depth influences features of subsurface flow such as the distribution of pathlines, velocity and residence time along these pathlines. While the incorporation of exponential decline in saturated hydraulic conductivity can be relatively straightforward for conceptual models (Beven, 1983; Beven, 1984), the step from conceptual boxes to a more explicit and detailed description of flow paths and residence times has been challenging. One notable exception is the multiple interacting pathways model (MIPs) suggested originally by Beven *et al.* (1989) and more recently developed by Davies *et al.* (2013). MIPs

*Correspondence to: Ali A. Ameli, Department of Biology, Biological & Geological Sciences Building, University of Western Ontario, London, Ontario, N6A 5B7 Canada.
E-mail: aameli2@uwo.ca

can represent both subsurface flow and particle transport in an 'integrated' solution, directly acknowledging exponential decline in K_s as well as small-scale (pore) and large-scale (e.g. preferential flow) subsurface heterogeneity.

The MIPs model, however, has many degrees of freedom (parameters) and requires the assumption of exponential water velocity distribution with porosity, which can be unrealistic under certain subsurface conditions. Other distributed watershed-scale conceptual models have taken this into account via a variable (albeit not exponential) saturated hydraulic conductivity with depth. Such work has resulted in prediction of mean transit time, but not explicit flow pathline and residence time distributions (e.g. Vaché and McDonnell, 2006). More recently, Birkel et al. (2011) used a novel lumped conceptual flow-tracer model to predict subsurface tracer composition and transit time using a simple linear discharge-storage relationship to calculate tracer composition in both soil and shallow groundwater reservoirs. An assumption of instantaneous and complete mixing at each reservoir is required, with many storage-related parameters to be calibrated. While useful, such reservoir and storage-based models cannot explicitly incorporate the potential impacts of the variation in saturated hydraulic conductivity with depth on subsurface flow and transport.

Discrete physically based numerical models offer an alternative approach with the potential to incorporate both an exponential decline in K_s (by adopting many discrete sublayers with different K_s) as well as an explicit subsurface flow and transport solution (e.g. Cardenas and Jiang, 2010). But the implementation of rapid changes in K_s with depth in free boundary models with a priori unknown location of water table may cause high computational cost and numerical difficulties (such as numerical instability, dispersion and artificial oscillation) for the particle transport solution, which are compounded as the rate of K_s change with depth increases. This problem can be attributed to the interpolation process that is required to generate a continuous map of subsurface velocity (from a 'discrete' map of potential head). This cannot always satisfy local mass balance, especially as the degree of heterogeneity in subsurface material properties increases. Salamon et al. (2006); Starn et al. (2012) and more recently Ameli and Abedini (2016) have commented on the limitations of discrete grid-based numerical subsurface transport models. Such schemes to date have considered gradual, smooth changes in K_s with depth (e.g. Jiang et al., 2009; Cardenas and Jiang, 2010; Jiang et al., 2010). But much more rapid changes in K_s with depth are the norm, especially in shallow glacial till catchments (e.g. Lundin, 1982; Nyberg, 1995; Seibert et al., 2011; Grip, 2015).

'Continuous' grid-free analytical models can offer a stable, efficient alternative to available numerical and conceptual schemes for simulation of subsurface flow and particle movement in hillslopes with an exponential decrease in saturated hydraulic conductivity with depth. These models have fewer degrees of freedom and rapidly produce continuous maps of velocity without any interpolation-related issues. In recent years, several such models have been presented that are able to explicitly (and continuously) incorporate an exponential depth-decaying saturated hydraulic conductivity function (Marklund and Wörman, 2007; Jiang et al., 2011; Wang et al., 2011; Zlotnik et al., 2011). Notwithstanding, traditional analytical solutions are restricted typically to geometrically simple groundwater systems and cannot be used for the purpose of subsurface flow and particle movement simulation in systems with a more realistic degree of complexity. Specifically, the existing analytical schemes (as well as many conceptual and numerical models) that include the exponential decline in saturated hydraulic conductivity have relied on a key assumption: that the topography represents the gradients in groundwater surface, i.e. topography-driven assumption (Toth, 1963). Such works treat the water table location as a replica of land surface either without the inclusion of the unsaturated zone (e.g. Cardenas and Jiang, 2010; Jiang et al., 2011; Wang et al., 2011) or with an unsaturated zone that the water table is a quasi-parallel of the land surface (e.g. Beven and Kirkby, 1979). The latter implies a uniform depth of the unsaturated zone [refer to Haitjema and Mitchell-Bruker (2005) as well as Marklund and Wörman (2011) for a general discussion on the limitations of this widely used assumption].

Clearly, treatment of the water table as an a priori unknown boundary (free boundary) in a coupled saturated-unsaturated solution would overcome the problems associated with the topographic assumption. Recently, Ameli and Craig (2014) and Ameli et al. (2013) have removed the geometrically simple and topography driven restrictions from analytical schemes and developed steady-state free boundary models to simulate 2D and 3D groundwater-surface water interaction in multi-layer naturally complex hillslopes. They accurately included the vadose, capillary fringe and ground water zones while a priori unknown location of the water table was determined iteratively. Here we extend the multi-layer approach presented by Ameli et al. (2013) to simulate 2-D free boundary fully coupled saturated-unsaturated flow in hillslopes with exponentially depth-decaying saturated hydraulic conductivity. This grid-free approach can provide the location of the water table elevation at different steady-state flow conditions. This solution exactly satisfies the saturated and unsaturated governing equations in the entire domain and explicitly takes into

account the exponential depth decay K_s. This solution immediately provides potential and velocity fields in the entire domain with no need for interpolation. This allows a continuous (rather than discrete as is common in numerical approaches) particle tracking scheme. Consequently, it opens up, for the first time, an approach for efficient exploration of the effect of different configurations in the exponential K_s decline on internal subsurface features such as flow pathlines, velocity and residence time distributions along these flow paths. The source and destination of each particle are also determined, along with the transit time distribution (TTD) of particles discharged into the stream. The objectives of this paper are therefore as follows:

1. Present a novel semi-analytical approach for an integrated simulation of subsurface flow and particle movement in hillslopes where K_s decays exponentially with depth.
2. Assess the effect of changing the rate of exponential decline in K_s with depth on flow pathlines, groundwater age and velocity distributions, as well as groundwater table location.
3. Demonstrate the effect of systematic heterogeneity in saturated hydraulic conductivity on the time-invariant TTD.

In addressing these questions, we build on recent experimental studies that have hypothesized that variation in the shape of TTD can be tied to large-scale heterogeneities in subsurface structure (e.g. Hrachowitz *et al.*, 2010). Our work is the first assessment of such hypotheses using a robust integrated flow and transport models that respects the subsurface architecture of catchments where decline in K_s with depth is rapid.

METHODS

Figure 1a depicts the general schematic of a shallow hillslope with an exponentially depth decaying saturated hydraulic conductivity. A hillslope with length L is located in the vicinity of a watercourse with a constant head of H_r. The bottom bedrock $z_b(x)$ and sides of the hillslope are impermeable, and the topographic surface ($z_t(x)$) is subject to a specified infiltration function ($R(x)$) together with a Dirichlet condition along surface water bodies (e.g. a watercourse with specified width and head). The saturated–unsaturated interface or top of the capillary fringe ($z_{CF}(x)$) is an *a priori* unknown boundary which defines both the location of the top of the saturated zone (including groundwater and capillary fringe zones) and the bottom of unsaturated zone. Hereafter, (s) and (u) denote saturated and unsaturated properties/variables. The *a priori* unknown water table ($z_{WT}(x)$) is also defined as a boundary with zero pressure head.

In a manner similar to e.g. Ameli *et al.* (2013) for the saturated zone the problem is posed in terms of a discharge potential, ϕ_s [$L^2 T^{-1}$], defined as

$$\phi_s(x, z) = K_{s0} h_s(x, z) \tag{1}$$

where $h_s(x, z)$ is the total hydraulic head and K_{s0} [LT^{-1}] is the saturated hydraulic conductivity along the topographic surface. Note that saturated hydraulic conductivity at each internal location (x, z) is defined as $K_s(x, z) = K_{s0} e^{\alpha(Z - Z_t(x))}$, where α is the parameter defining the exponential relationship between saturated hydraulic conductivity and depth. A positive α value generates a depth-decaying exponential relationship between saturated hydraulic conductivity and depth (Figure 1b).
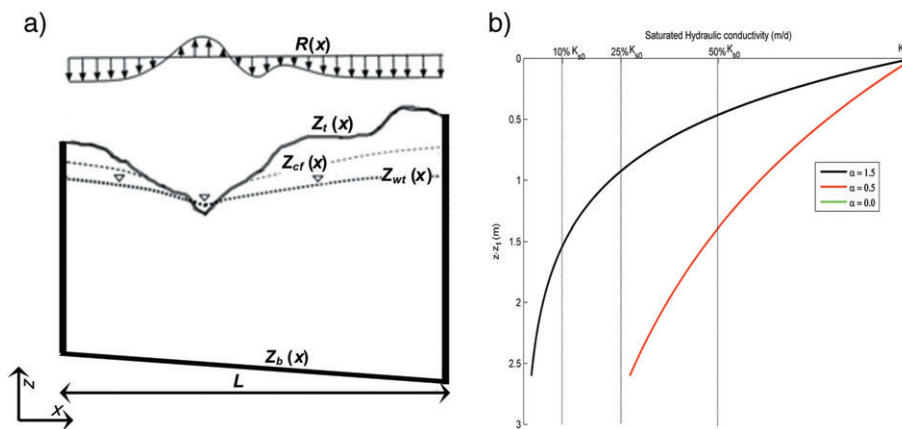

Figure 1. General schematic of a shallow hillslope with an exponentially depth decaying saturated hydraulic conductivity. (a) hillslope layout, (b) the exponential relationship between saturated hydraulic conductivity and depth where K_{s0} [LT^{-1}] is the saturated hydraulic conductivity along the topographic surface (Z_t). α is the parameter defining the exponential relationship between K_s and soil depth (i.e. $Z - Z_t$). $\alpha = 0$ refers to the homogenous K_s over the entire soil depth profile. Z_{WT} and Z_{CF} refer to the water table and top of the capillary fringe interfaces respectively. The sides of the domain and bottom bedrock (Z_b) are assumed as impermeable interfaces

Mathematical formulation

Using continuity of mass, Darcy's law and an exponentially declining relationship between saturated hydraulic conductivity and depth, the saturated discharge potential function (ϕ_s) must satisfy the following Helmholtz equation:

$$\frac{\partial^2 \phi_s}{\partial x^2} + \alpha \frac{\partial \phi_s}{\partial z} + \frac{\partial^2 \phi_s}{\partial z^2} = 0 \tag{2}$$

This equation is based on the assumption that K_s is only the function of z and does not change with x direction at each z elevation (K_{s0} should be constant along a horizontal datum). To remove this restriction and implement constant K_{s0} along the topographic surface and not a horizontal datum, we use a coordinate transform scheme [similar to Craig (2008)] to ensure an exact implementation of exponential decline in K_s with soil depth. For the vadose zone, exponential Gardner's constitutive function (Gardner, 1958) with an air entry pressure of (φ^e) and Gardner's sorptive number of β [L^{-1}] is used to define the relationship between unsaturated hydraulic conductivity (K_u) and pressure head (φ) as

$$K_u(\varphi, x, z) = K_s(x, z) e^{(\beta(\varphi - \varphi^e))} \tag{3}$$

Sorptive number refers to the relative significance of gravitational compared with capillary forces (Philip, 1957). This number can be obtained experimentally for each soil by fitting Gardner's model to observed suction – hydraulic conductivity (or saturation) data. The implementation of a vadose zone solution in terms of a Kirchhoff potential ϕ_u [L^2T^{-1}] accompanied by the Gardner relationship [Equation (3)], facilitate the linearization process of the nonlinear Richards Equation [refer to Ameli *et al.* (2013) and Bakker and Nieber (2004) for more detail]. Here, at each coordinate (x, z), the Kirchhoff potential is a function of pressure (suction) head φ [L] as

$$\phi_u(\varphi) = \int_{-\infty}^{\varphi} K_{s0}\ e^{(\beta(\eta - \varphi^e))}d\eta \quad \varphi < \varphi^e \tag{4}$$

$$\phi_u(\varphi) = \frac{K^e}{\beta}\exp(\beta\varphi) \tag{5}$$

where $K^e = K_{s0}\exp(-\beta\varphi^e)$ [LT^{-1}]. Now from the non-linear steady-state form of Richards' equation,

$$\frac{\partial}{\partial x}\left(K_u\frac{\partial\varphi}{\partial x}\right) + \frac{\partial}{\partial z}\left(K_u\frac{\partial\varphi}{\partial z}\right) + \frac{\partial}{\partial z}K_u(\varphi) = 0 \tag{6}$$

and given the Equation (3) for K_u and Equation (4) for ϕ_u, we can derive an equivalent linear 2D governing equation for the vadose zone in terms of Kirchhoff potential:

$$\frac{\partial^2 \phi_u}{\partial x^2} + \frac{\partial^2 \phi_u}{\partial z^2} + (\alpha + \beta)\frac{\partial \phi_u}{\partial z} + (\alpha\beta) \phi_u = 0 \tag{7}$$

Again, the previously mentioned equation is based on the assumption of a constant saturated hydraulic conductivity (K_{s0}) along a horizontal datum. This limitation in representing a constant K_{s0} that follows the ground surface is overcome here as well through coordinate transformation. Although the K_s exponentially varies with depth, a uniform Gardner's sorptive number (β) and air entry pressure is assumed for the entire unsaturated domain. This assumption is common in development of unsaturated models in multi-layer or exponentially varying K_s systems (e.g. Srivastava and Yeh, 1991; Warrick and Knight, 2003; Warrick *et al.*, 2008). Across the sides of the domain in both unsaturated and saturated zones, no-flow conditions in the *x*-direction are imposed (Figure 1a) as

$$\frac{\partial\phi_u}{\partial x}(0, z) = 0 \tag{8a}$$

$$\frac{\partial\phi_u}{\partial x}(L, z) = 0 \tag{8b}$$

$$\frac{\partial\phi_s}{\partial x}(0, z) = 0 \tag{8c}$$

$$\frac{\partial\phi_s}{\partial x}(L, z) = 0 \tag{8d}$$

where L is the domain length. The topographic surface is subject to an arbitrary (but predefined) infiltration–evapotranspiration function $R(x)$ [LT^{-1}]:

$$\frac{\partial\phi_u}{\partial\eta}(x, z_t(x)) = R(x) \tag{9}$$

$R(x)$ is taken as positive for infiltration and negative for evapotranspiration. The solution derived herein can be used in combination with any arbitrary infiltration/evapotranspiration function [as shown by Ameli *et al.* (2013)]; however, we consider a uniform infiltration for the test cases assessed in this paper. At the surface of a watercourse a uniform hydraulic head (H_r) is applied and along the bottom bedrock, a no-flow condition is imposed as

$$\frac{\partial\phi_s}{\partial\eta}(x, z_b(x)) = 0 \tag{10}$$

Furthermore, continuity of flux and pressure head must be enforced along the boundary between unsaturated and

saturated zones, i.e. the top of capillary fringe (Z_{CF} in Figure 1a):

$$\frac{\partial \phi_u}{\partial \eta}\left(x, z_{\text{cf}}^-(x)\right) = \frac{\partial \phi_s}{\partial \eta}\left(x, z_{\text{cf}}^+(x)\right) \quad (11)$$

$$\frac{\phi_s}{K_s(x, z_{\text{cf}}(x))}\left(x, z_{\text{cf}}^+(x)\right) - z_{\text{cf}}^+(x) = \varphi_u\left(x, z_{\text{cf}}^-(x)\right) = \varphi^e \quad (12)$$

In Equations, (9) to (11), η is the coordinate normal to each surface which is either the topographic surface, $z_t(x)$, bottom bedrock, $z_b(x)$, or the top of capillary fringe $z_{\text{cf}}(x)$. The normal first order derivative ($\frac{\partial \phi}{\partial \eta}$) along these surfaces would be decomposed into vertical and horizontal components [refer to Ameli and Craig (2014) for more detail].

Using the separation of variables method and in a manner similar to Wang *et al.* (2011) the general series solution to the saturated governing equation [Equation (2)] with no-flow conditions along the sides of the saturated domain [Equations (8c) and (8d)] is obtained as

$$\phi_s(x, z) = A_0 + \sum_{n=1}^{N}\left(A_n\left[\cos\left(\frac{n\pi}{L}x\right)\exp(\gamma_n z)\right] \right. \quad (13)$$
$$\left. + B_n\left[\cos\left(\frac{n\pi}{L}x\right)\exp(\bar{\gamma}_n z)\right]\right)$$

where $\gamma_n = \frac{-\alpha}{2} + \frac{1}{2}\sqrt{\alpha^2 + \left(\frac{2n\pi}{L}\right)^2}$, $\bar{\gamma}_n = \frac{-\alpha}{2} - \frac{1}{2}\sqrt{\alpha^2 + \left(\frac{2n\pi}{L}\right)^2}$

In Equation (13), N is the total number of terms in the series solution, n represents the coefficient index and A_n, B_n are the unknown series coefficients associated with the nth coefficient index. Similarly, the general series solution to the unsaturated governing equation [Equation (7)] is obtained as

$$\phi_u(x, z) = C_0[\exp(-\beta z)] \quad (14)$$
$$- \sum_{m=1}^{M}\left(C_m\left[\cos\left(\frac{m\pi}{L}x\right)\exp(\pounds_m z)\right]\frac{\pounds_m}{\frac{m\pi}{L}}\right.$$
$$\left. + D_m\left[\cos\left(\frac{m\pi}{L}x\right)\exp(\overline{\pounds}_m z)\right]\frac{\overline{\pounds}_m}{\frac{m\pi}{L}}\right)$$

where $\pounds_m = \frac{-(\alpha+\beta)}{2} + \frac{1}{2}\sqrt{(\alpha+\beta)^2 - 4\alpha\beta + \left(\frac{2n\pi}{L}\right)^2}$, $\overline{\pounds}_m = \frac{-(\alpha+\beta)}{2} - \frac{1}{2}\sqrt{(\alpha+\beta)^2 - 4\alpha\beta + \left(\frac{2n\pi}{L}\right)^2}$

In the above equation, M is the total number of series terms, m refers to the coefficient index and C_m, D_m are the unknown series coefficients associated with the mth coefficient index.

The unknown coefficients (A_n, B_n and C_m, D_m) are calculated to complete the potential solutions [Equations

(13) and (14)]. These coefficients are obtained by imposing the continuity and boundary conditions [Equations (9–12)] along associated interfaces (topographic surface, bottom bedrock and the top of capillary fringe). To impose these conditions, a least squares numerical algorithm is applied at a set of evenly-spaced control points (NC) located along the previously mentioned interfaces. The *a priori* unknown top of the capillary fringe interface, $z_{CF}(x, y)$, is obtained through a robust iterative scheme [for details of the iterative scheme readers are referred to Ameli *et al.* (2013)]. The water table elevation, $z_{WT}(x, y)$, is then located as an interface with zero pressure head.

Particle tracking and residence times

Derivatives of Equation (13) with respect to x and z provide a continuous field of Darcy fluxes in x ($q_{sx}(x, z)$) and z ($q_{sz}(x, z)$) directions throughout the entire saturated zone. Darcy–Buckingham fluxes in the unsaturated zone can also be obtained as follows

$$q_{ux}(x, z) = e^{\alpha(z - Z_t(x))}\frac{d\phi_u(x, z)}{dx} \& q_{uz}(x, z)$$
$$= e^{\alpha(z - Z_t(x))}\left[\frac{d\phi_u(x, z)}{dz} + \beta\phi_u(x, z)\right] \quad (15)$$

Continuous fields of pore velocity in x and z directions are subsequently obtained by dividing Darcy and Darcy-Buckingham fluxes by moisture content. In the saturated zone, the moisture content is equal to the saturated moisture content (porosity), which is assumed as 0.50 for the test cases assessed in this paper. In the unsaturated zone, moisture content is obtained based on the suction pressure head at each location. The calculated continuous fields of pore velocity (in both directions and both zones) are then used to track particles and generate pathlines from the topographic surface to the water course using a Runge Kutta algorithm. Here, we only consider the effect of advective particle movement, although the proposed particle tracking method is also flexible to take into account the effects of dispersion and diffusion.

The simulated pathlines are then employed to obtain time invariant advective groundwater age and transit time. Here, the simulated transit times are fitted by a Gamma distribution to obtain the hillslope TTD. The expression for the Gamma distribution probability density function (pdf) can be expressed as a function of the transit time (τ) as

$$p(\tau) = \frac{\tau^{a-1}}{b^a \Gamma(a)}e^{-\frac{\tau}{b}} \quad (16)$$

where b is a scale parameter, a is a Gamma shape parameter and Γ is the Gamma function. Note that the product of a and

b represents the mean transit time (τ_0). Many numerical and/or experimental studies have suggested that Gamma distribution can appropriately emulate the behaviour of short and long term time invariant TTDs compared with the other models (Kirchner *et al.*, 2000; Fiori and Russo, 2008; Hrachowitz *et al.*, 2009; Godsey *et al.*, 2010). As the Gamma shape parameter (a) varies, additionally, this distribution can represent (and approximate) other distributions that are used for the purpose of determination of TTD. For example, as a approaches 1, the Gamma distribution represents an exponential distribution ($p(\tau) = \frac{1}{b}e^{-\frac{\tau}{b}}$). Gamma distributions with a Gamma shape parameter in the range between 0.25 to 0.75 can exhibit a fractal scaling behaviour (Gisiger, 2001) and as the shape parameter approaches 0.5 this fractal behaviour becomes stronger (Kirchner *et al.*, 2001). Gamma distributions also approximate power law distributions [$p(\tau) \approx \tau^{a-1}$] with the advantage that the gamma distribution is integrable at large transit times; the power law distribution may exhibit an infinite mean groundwater age (e.g. Kirchner *et al.*, 2000; Cvetkovic and Haggerty, 2002). Gamma distribution is also more efficient than two parallel linear reservoir models (Weiler *et al.*, 2003) because the flow partitioning does not have to be known *a priori*.

MODEL ASSESSMENT AND APPLICATION

In this section we assess the numerical behaviour of the semi-analytical series solution method for the simulation of saturated-unsaturated flow in a hypothetical hillslope. The saturated and unsaturated governing equations [Equations (2) and (7)] as well as the exponential decline in K_s with depth are met exactly in the present scheme, but the boundary conditions [Equations (9–12)] are imposed using a numerical least square algorithm subject to numerical error. Imposing boundary conditions also leads to the determination of unknown coefficients of the saturated and unsaturated series solutions [Equations (13) and (14)]. Therefore, we start by assessing the numerical error in the implementation of boundary conditions. We then go on to examine the impact of changing the rate of decline in K_s with soil depth on groundwater table location, flow pathlines, velocity, groundwater age and TTDs.

The hillslope application

We developed a series solution for simulation of 2D saturated-unsaturated flow in a hypothetical shallow till hillslope where the saturated hydraulic conductivity declines exponentially with depth (Figure 2c). The saturated hydraulic conductivity along the topographic
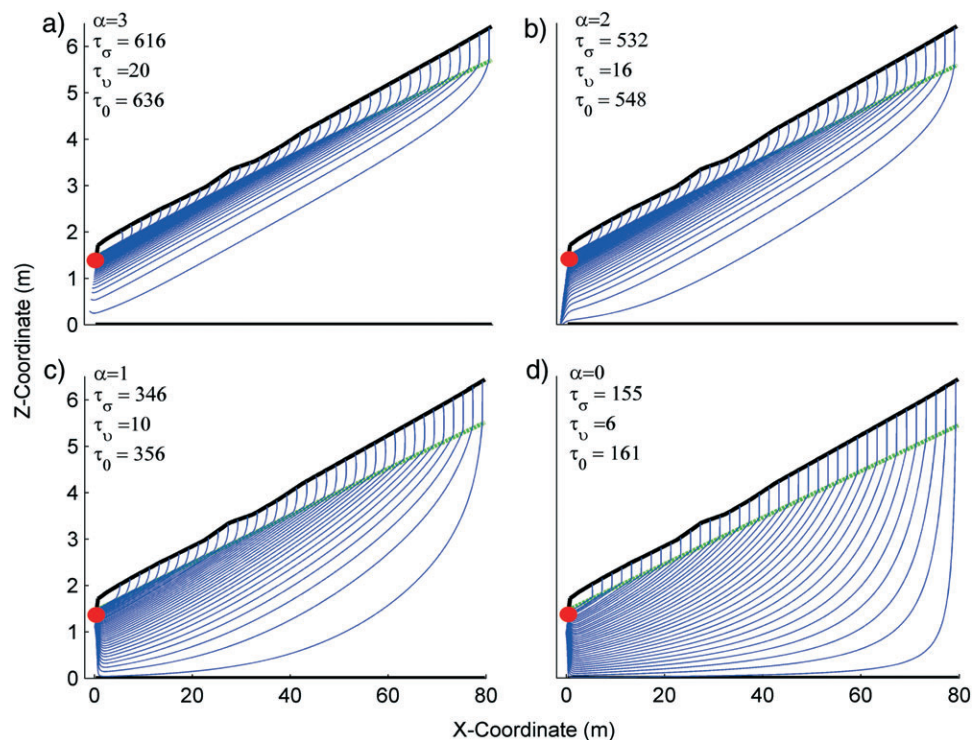

Figure 2. Flow pathline distribution and water table (green dashed line) interface, and groundwater age for different rates in the exponential decline of K_s (α). (a) $\alpha = 3$, (b) $\alpha = 2$, (c) $\alpha = 1$ and (d) $\alpha = 0$ (homogenous case). τ_σ, τ_υ and τ_0 represent mean groundwater age (day) in saturated, unsaturated zones and entire hillslope respectively. The watercourse is located at the left side of the domain within the red circle. The no-flow boundary at the bottom is located at $Z_b = 0$

surface (K_{s0}) was set to 60 m/day and the exponential parameter representing the relationship between saturated hydraulic conductivity and depth was assumed as $\alpha = 1\frac{1}{m}$. The unsaturated hydraulic conductivity properties [Equation (3)] including air entry pressure (φ^e) and Gardner's parameter (β) were set to -0.05 m and $0.25\frac{1}{m}$ respectively. An average porosity equal to 0.50 was considered for the entire domain; this was used for the purpose of obtaining pore velocity from Darcy and Darcy-Buckingham fluxes [Equation (15)]. An infiltration rate of $R = 1.5 \times 10^{-3}$ m/day was considered, which is identical to the subsurface discharge rate to the stream for this steady-state analysis. The hillslope length (distance from stream to water divide) and average angle were 80 m and 5% respectively. The assumed hillslope geometry, hydrological and hydrogeological properties used for this hypothetical example can be found in the boreal/hemiboreal landscape of Canada, Fennoscandia and many other places. Along the watercourse located at the left of the domain (Figure 2c), a uniform head of $H_r = 1.45$ m was established. The least square solution was obtained using $NC = 160$ evenly spaced control points per interface (z_t, z_b and z_{CF} in Figure 1a). For the saturated zone solution [Equation (13)] and unsaturated zone solution [Equation (14)], a small number of series terms of $N = 140$ and $M = 140$ respectively were used [in total 562 ($2N + 1 + 2M + 1$)]. After 50 iterations the model has converged on the location of the a priori unknown top of the capillary fringe interface. The water table was also defined as an interface of zero pressure head (green dashed lines in Figure 2c).

Boundary condition assessment

Here, the least square errors in boundary conditions [Equations (9–12)] are evaluated along each interface at points located halfway between the control points used within the least squares solution as follows:

$$\varepsilon_t^{\text{flux}}(x) = \frac{\frac{\partial \phi_u}{\partial \eta}(x, z_t(x)) - R}{R} \tag{17a}$$

$$\varepsilon_b^{\text{flux}}(x) = \frac{\frac{\partial \phi_s}{\partial \eta}(x, z_b(x))}{R} \tag{17b}$$

$$\varepsilon_{CF}^{\text{flux}}(x) = \frac{\frac{\partial \phi_u}{\partial \eta}(x, z_{\text{cf}}^-(x)) - \frac{\partial \phi_s}{\partial \eta}(x, z_{\text{cf}}^+(x))}{R} \tag{17c}$$

$$\varepsilon_{CF}^{\text{head}}(x) = \frac{\varphi_u(x, z_{\text{cf}}^-(x)) - \varphi^e}{H_r} \tag{17d}$$

$\varepsilon_t^{\text{flux}}$, $\varepsilon_b^{\text{flux}}$ and $\varepsilon_{CF}^{\text{flux}}$ refer to normalized (with respect to infiltration rate) least square flux error along the topographic surface (z_t), bottom bedrock (z_b) and the *a priori* unknown top of the capillary fringe (z_{CF}) interfaces respectively. The $\varepsilon_{CF}^{\text{head}}$ also refers to the normalized (with respect to watercourse head) least square head error along the top of the capillary fringe (z_{CF}) interface. These errors were within acceptable ranges with a maximum of 5×10^{-4}, 5×10^{-5}, 6×10^{-8} and 5×10^{-6} for $\varepsilon_t^{\text{flux}}$, $\varepsilon_{CF}^{\text{flux}}$, $\varepsilon_{CF}^{\text{head}}$ and $\varepsilon_b^{\text{flux}}$ respectively (Figure 3). Here, a maximum of
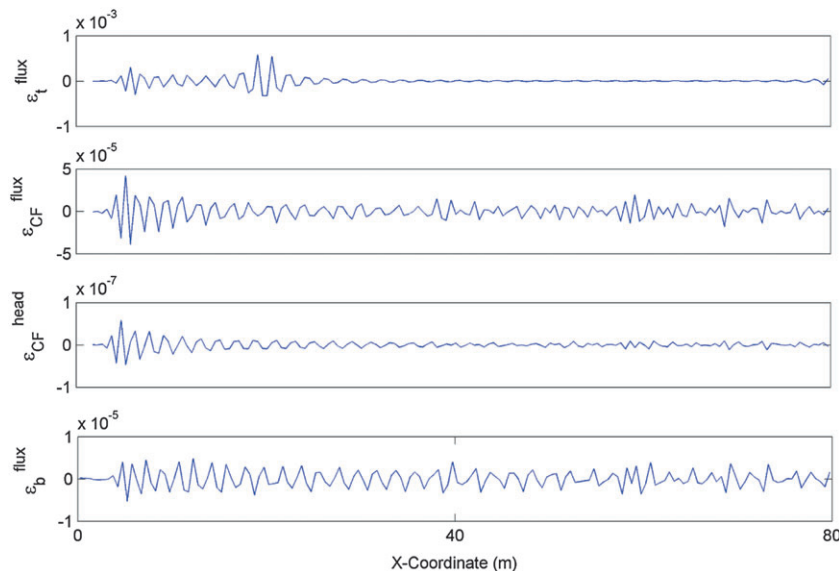

Figure 3. The normalized error at 160 points located across each boundary interface. $\varepsilon_t^{\text{flux}}$ refers to the normalized flux error in topographic surface boundary condition, $\varepsilon_{CF}^{\text{flux}}$ is the normalized error in the continuity of flux along the top of capillary fringe, $\varepsilon_{CF}^{\text{head}}$ represents the normalized error in the continuity of head along the top of capillary fringe and $\varepsilon_b^{\text{flux}}$ refers to the normalized error along the bottom bedrock boundary condition. Flux errors were normalized with respect to infiltration rate and head errors were normalized with respect to water course head

5×10^{-4} (0.05%) normalized flux error along the topographic surface means that more than 99.95% of the desired infiltration rate (i.e. 1.5×10^{-3} m/day) meets along this interface. The least square errors also resemble a white noise which implies that there is not any specific trend in these errors.

Impact of systematic heterogeneity in K_s on subsurface flow characteristic

The model was used to illustrate the impact of changing the rate of decline in K_s with depth on the groundwater table location, flow pathlines, velocity, groundwater age and dimensionless TTDs. Different α values equal to 0 (homogenous case), $1 \frac{1}{m}$ (original case study), $2 \frac{1}{m}$ and $3 \frac{1}{m}$ were used while the remaining parameters were the same as in the original example (Figure 2). Given an identical saturated hydraulic conductivity of $K_{s0} = 60$ m/day along the topographic surface, the more rapidly K_s declines (i.e. the larger the value of α), the more nearer the surface the water table elevation becomes. There is also an increase in deviation from verticality of flow in the unsaturated zone. Deep circulation further away from the watercourse is reduced, generating fewer flow pathlines in the deeper portions of the hillslope near the water divide. Superficial flow in the vicinity of the watercourse (the discharge area) increases because the water table is raised to reach the higher saturated hydraulic conductivity closer to the topographic surface. The mean groundwater age in both the saturated and unsaturated zones (and therefore in total) also increases as the rate of decline in K_s with depth increases. The rate of increase in mean groundwater age is more pronounced in the saturated zone compared with the unsaturated zone which can be attributed to a decrease in unsaturated zone thickness as α increases.

The rate of decline in K_s also affects the particle pore (relative) velocity distribution (Figure 4). This effect on saturated zone velocity is complex and varies depending upon the distance from the watercourse. For the case of homogenous K_s ($\alpha = 0$), saturated velocity increases smoothly (and uniformly with depth) towards the water course (Figure 4d). As α increases, the saturated zone relative velocity increases sharply (and non-uniformly with depth) towards the water course. The proportion of the saturated aquifer with a very small relative velocity also increases (this slow moving water is found far from the stream at depth). Furthermore, the saturated relative velocity in discharge area near the watercourse is uniform with depth for the case of homogenous K_s and decreases with depth as α increases. In other words, systematic declines in K_s with depth increases the velocity of shallow flow relative to flow deeper in the soil profile in both the vicinity of the watercourse and further away. The rate of K_s decline does not affect unsaturated (relative) velocity substantially. Given an identical saturated hydraulic conductivity along the topographic surface for all α values, at a specific depth in the unsaturated zone, saturated hydraulic conductivity is lower for a larger α; however, this may be nullified by higher moisture
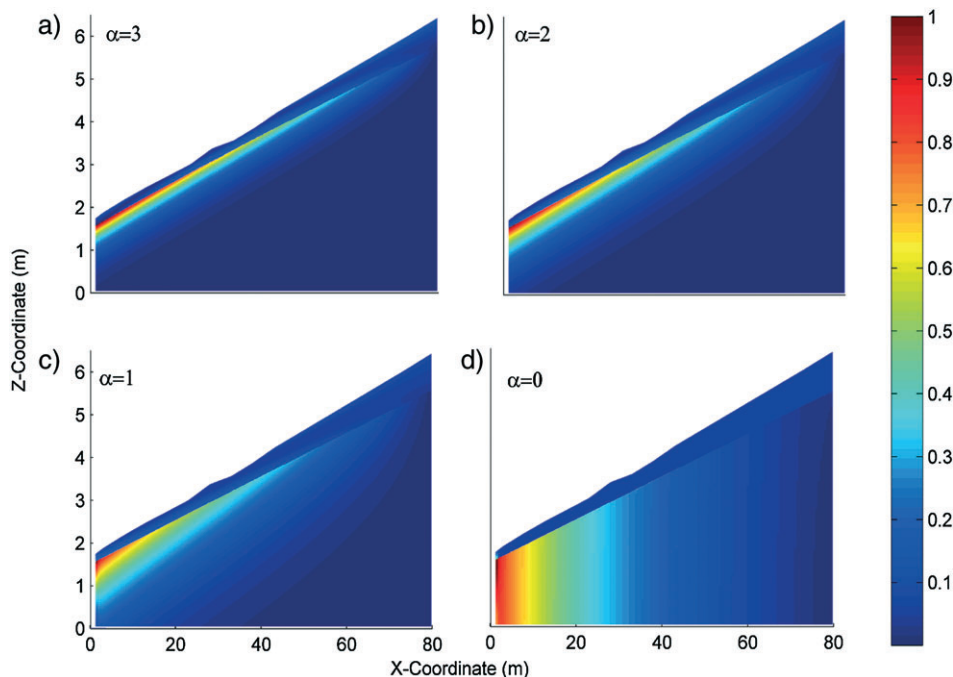

Figure 4. Effect of systematic exponential decline in K_s with depth on the relative velocity distribution of flow particles. (a) $\alpha = 3$, (b) $\alpha = 2$, (c) $\alpha = 1$ and (d) $\alpha = 0$. In each figure, velocities were normalized with respect to the maximum velocity

content, and therefore, higher unsaturated hydraulic conductivity at this depth because the water table elevation is higher for a larger α (as shown in Figure 2).

Groundwater age patterns are a manifestation of flow pathlines and velocity distributions, which are both affected by how quickly the saturated hydraulic conductivity decreases (Figure 5). Indeed as the rate of K_s change with depth increases, there is a systematic increase in the disparity of the groundwater age across the hillslope including groundwater age reaching the watercourse. The 'tail' of older groundwater is found further from the stream and at greater depths.

The increasing disparity in velocity and ages of the water as α increases is reflected in the fitted transit time pdf for water in the unsaturated zone (Figure 6a), the saturated zone (Figure 6b) and the entire hillslope (Figure 6c). The variability of transit times relative to mean unsaturated groundwater age (τ_v) decreases as α increases; this is because of the fact that the thickness of unsaturated zone becomes more uniform (Figure 6a). In the saturated zone, the dimensionless transit time pdf exhibits a sharper decay at the shorter transit time end of the distribution with a more prominent tail of older water as α increases (Figure 6b). In other words, the frequency of both very young and very old water increases. The mean saturated transit time (τ_σ) also increases from 155 to 616 days (Figure 2).

In the entire hillslope the dimensionless pdf of the fitted transit times indicates that the percentage of both young and old waters increases with an increase in the rate of K_s decline with depth (Figure 6c). For the range of α values considered here the TTD of the entire hillslope is almost similar to that of saturated zone. Furthermore, the Gamma shape parameter decreases from 0.90 for the homogenous case ($\alpha = 0$) to 0.51 for the most rapid decline in K_s ($\alpha = 3$); this suggests that the TTD of the entire hillslope varies from (almost) exponential distribution to a general Gamma distribution with a fractal behaviour as systematic exponential decline in K_s with depth increases. The mean transit time in the entire hillslope also increases from 161 to 636 days with rates almost similar to the saturated zone mean transit time (Figure 2).

DISCUSSION

This paper presented and employed a new grid-free semi-analytical method for simulating saturated-unsaturated flow and particle movements in hillslopes where there is an exponential decrease in saturated hydraulic conductivity (K_s) with soil depth. The real usefulness of this steady-state solution *versus* available analytical, numerical and conceptual models for catchments characterized by this type of subsurface soil architecture is that this integrated flow and transport scheme breaks from the topography-driven assumption (i.e. the water table and the hydraulic gradient of the saturated zone follow the slope of the topography) by allowing the calculation of an
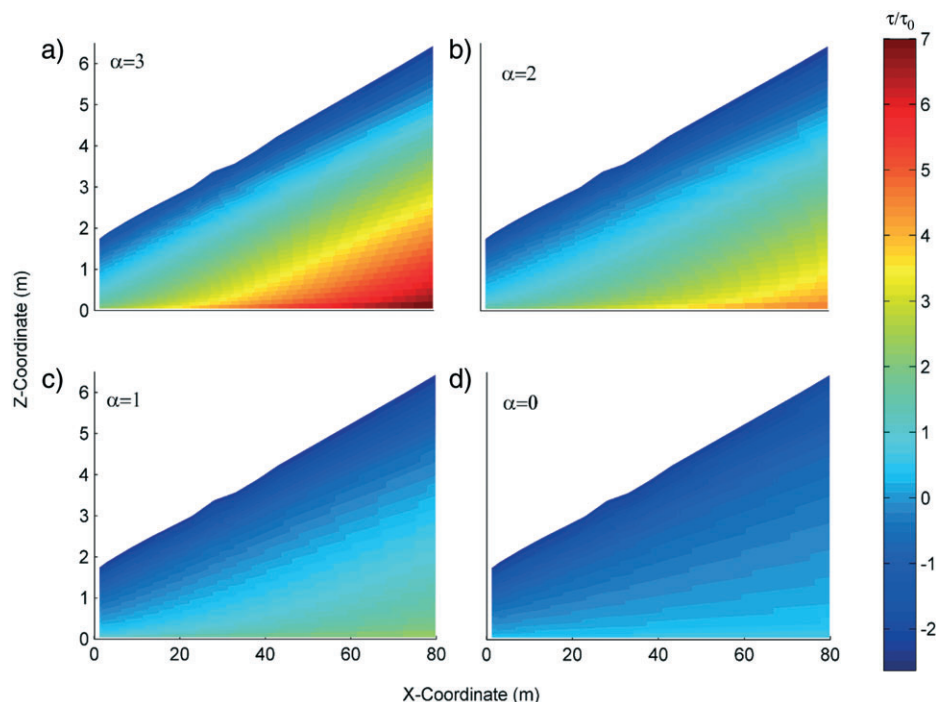

Figure 5. Effect of the rate of K_s exponential decrease with depth on groundwater age pattern. (a) $\alpha = 3$, (b) $\alpha = 2$, (c) $\alpha = 1$ and (d) $\alpha = 0$ (homogenous case). Ages (τ) are normalized with respect to τ_0 which refers to mean groundwater age corresponding to each α value
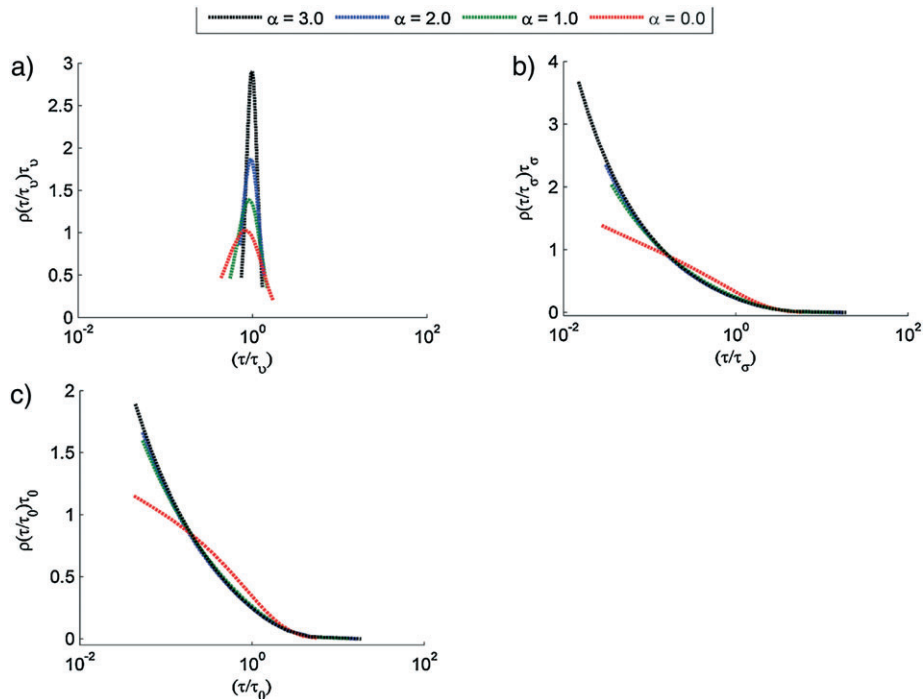
Figure 6. Effect of systematic exponential decline in K_s with depth on dimensionless travel time probability density function. (a) unsaturated zone, (b) saturated zone and (c) entire hillslope

a priori unknown water table location and capillary fringe. This solution exactly and efficiently satisfies the continuity of mass, as well Darcy's law in the saturated zone and Darcy–Buckingham's law in the unsaturated zone; albeit under the assumption that Gardner's model can emulate the suction-hydraulic conductivity behaviour in the unsaturated zone.

In our application of the model, a wide range in the exponential relationship (α) between saturated hydraulic conductivity (K_s) and soil depth were simulated, from the case of a uniform soil profile ($\alpha = 0$) to a strong heterogeneity ($\alpha = 3$). This approach can quickly (without any interpolation process as is common in discrete numerical approaches) provide continuous potential and particle velocity fields, consistent with the degree of heterogeneity, within the entire hillslope. This can be used in an integrated flow and transport modelling framework to efficiently track the particles, generate flow pathlines, define the sources and the residence time of each particle at each location within the hillslope and determine the TTD. These are all key factors in describing catchment hydrology and improving our understanding of hydrological processes (Hewlett and Troendle, 1975; McDonnell and Beven, 2014). The integrated flow and transport semi-analytical method presented here has great potential for efficient exploring the major controls on subsurface flow and supporting the formulation of hypotheses about system functioning in catchments where a rapid decline in K_s with depth challenges other models.

Steady-state assumption

The conceptual, numerical and analytical models that include a representation of the effect of exponential decline in K_s, typically employ a steady-state assumption (e.g. Cardenas and Jiang, 2010; Jiang *et al*., 2010; Zlotnik *et al*., 2011) or assume a succession of steady-state situation for groundwater level variations (e.g. Beven and Kirkby, 1979; Seibert, 1999). The solution presented in this paper is also makes this assumption. We know that subsurface flow and TTD are by nature time variant (Hrachowitz *et al*., 2010; Botter *et al*., 2011; Rinaldo *et al*., 2011; Botter, 2012; Klaus *et al*., 2015), and vary with wetness condition (Heidbüchel *et al*., 2013) as well as precipitation regime (Sayama and McDonnell, 2009). The limitations of the steady-state assumption need to be recognized, and a time variant version of this semi-analytical integrated flow and transport model would be desirable. In the future this might be accomplished by adding a Laplace Transform simulator (Bakker, 2013) to the present solution. Notwithstanding, we believe that the benefits of the grid-free method presented here justify use of this current steady-state version of the semi-analytical solution in the simulation of catchment–water course interactions in till-mantled environments. Seibert *et al*. (2003a) has shown that the groundwater level- discharge relationship can approximate a steady-state condition within tens of metres of the stream channel in glacial till hillslopes where transmissivity feedback controls the

subsurface flow. Additionally, the storage in the unsaturated zone can often be close to a steady-state with the water table (Seibert *et al.*, 2003b). This steady-state model is thus a good point of departure for an efficient exploring the behaviour of flow systems that have been difficult to model using the grid-based numerical scheme; albeit the latter has the potential to simulate transient flows. Furthermore, the time invariant TTD may still be valid for humid catchments (where seasonal rainfall variation is less significant) and/or if one focuses on long term behaviour of the catchment (Botter *et al.*, 2010; Hrachowitz *et al.*, 2010).

Modelling of flow paths, residence time and velocity

The integrated flow and transport semi-analytical series solution revealed the decisive influence of the rate of systematic decline in K_s on the internal characteristics of a hillslope in terms of groundwater age, velocity and flow paths patterns. As the rate of decline in K_s increases, a systematic ageing occurs in the entire hillslope, together with a broader range of ages. The groundwater discharging into the water course also becomes older. Our example results also show that the rate of K_s decline with depth (α) influences the velocity pattern, with a dependence on the distance to the stream. The effect of α on the unsaturated zone velocity is much smaller than in the shallow saturated portion of the aquifer. The effect of α is strongest in the vicinity of the water course in the superficial layers of the saturated zone where flow rates increase markedly as α increases. Our results also suggest a pronounced focusing of lateral flows to the most superficial layers of the saturated soil as the rate of decline in K_s with depth increases; this also corroborates with the findings of Weyman (1973). This behaviour has been hypothesized as a feature of the transmissivity feedback mechanism in glacial till hillslopes where K_s declines exponentially with depth, but this is the first time that the implications have been quantified for the entire hillslope flow system where the requirements for the conservation of mass have been satisfied.

Transit time distribution

The transit time of subsurface water from ground surface to the stream determines the type and rate of many processes occurring in surface, near surface and deep environments (Pinay *et al.*, 2015). The variability of transit times relative to mean groundwater age reveals the variability of flow pathlines and velocity distribution within the subsurface (Godsey *et al.*, 2010). The variability of transit times can be quantified by the shape parameter of the TTD. This parameter decreases as the variability increases. As stated earlier, the Gamma distributions with a Gamma shape parameter in the range

between 0.25 and 0.75 demonstrates a fractal scaling behaviour (Gisiger, 2001), and this fractal behaviour becomes stronger as the shape parameter approaches 0.5 (Kirchner *et al.*, 2001). Godsey *et al.* (2010) used spectral analysis on the long term tracer time series of 22 catchments in North America and Europe to calculate Gamma distribution shape parameters and found values ranging from 0.35 to 0.78. They also suggested that the widely used exponential distribution of TTD (with Gamma shape parameters equal to 1) cannot emulate the behaviour of these catchments. Hrachowitz *et al.* (2009) also reported a Gamma parameter of 0.5 for the Loch Ard catchment in Wales where transmissivity feedback controls subsurface flow. This parameter was reported as 0.77 in steady-state numerical analysis performed by Fiori and Russo (2008) in a mildly heterogeneous domain.

A few experimental and numerical analyses hypothesized that the variation of the Gamma shape parameter can be attributed to large-scale heterogeneities in subsurface structure (Fiori and Russo, 2008; Hrachowitz *et al.*, 2009; Hrachowitz *et al.*, 2010). However, this hypothesis has not been rigorously evaluated using an integrated flow and transport simulation except for a few cases where subsurface heterogeneity has implicitly been considered by imposing a large dispersion coefficient (Kirchner *et al.*, 2001; Kollet and Maxwell, 2008). The present study that simulates explicitly the effect of a systematic decline in saturated hydraulic conductivity with depth on saturated and unsaturated TTDs corroborates the earlier indications and speculations that K_s variation has a decisive impact on the TTD. Our results show that as the rate of change in hydraulic conductivity increases with depth (i.e. as α increases from 0 to 3), the fitted shape parameter of Gamma distribution in the entire hillslope varies from 0.90 to 0.51. This implies that TTD varies from an approximate exponential toward a strong fractal behaviour. Indeed, the greater the saturated hydraulic conductivity contrast (α) is, the smaller the value of the Gamma shape parameter becomes. This is associated with greater the spatial variability of groundwater age, velocity and flow pathlines inside the catchment. The conductivity contrast is related to the presence of macropores (e.g. Beven and Germann, 2013), recurring superficial soil frost and impermeable (or low permeable) bedrock underlying the permeable soil (e.g. Ameli *et al.*, 2015) that create a large-scale, systematic heterogeneity in the hydraulic conductivity of a natural hillslope. Our results also suggest that the Gamma shape parameter can be a good metric to determine the relative degree of soil heterogeneity (i.e. decline of k_s with depth) in contrasting catchments where time series of tracer concentration are available to enable an estimate of the TTD. The current study also shows that as the rate of decline in saturated hydraulic conductivity increases, the

behaviour of the transit time of the entire hillslope approaches the behaviour of the saturated zone transit time. This finding is in agreement with the numerical experiment of Kollet and Maxwell (2008). This may suggest that future models built for the purpose of explicit determination of TTD may not need to take into account the unsaturated zone in heterogeneous hillslopes with shallow groundwater tables. This is useful because inclusion of the unsaturated zone with non-linear behaviour can be challenging for physically based numerical and analytical models.

CONCLUSION

This paper presents a novel continuous grid-free approach for efficiently and explicitly calculating the internal catchment subsurface flow features (flow path line, residence time and TTD) where the saturated hydraulic conductivity profile changes exponentially with depth. Keith Beven's early work was among the first to recognize this importance, but it has been difficult to efficiently incorporate an exponential decline in saturated hydraulic conductivity with soil depth, together with an integrated flow and transport solution. The use of our new analytical model to explore the implications of rapid decline in saturated hydraulic conductivity with depth reveals how important this is for key features of catchment response. These include a focusing of lateral flow through the superficial saturated soils in the riparian zone and alteration of the tails in the TTD to allow for larger proportions of both much younger and older water. The efficiency of this model opens up new possibilities for exploring the role of catchment soil architecture on the flow paths and residence times of water in an important class of catchments with shallow flow systems in unconsolidated materials. The major limitation of the approach we present here is that it is a steady-state representation. Nevertheless, this is an exciting starting point for inquiry that uses analytical models to create and test hypotheses of flow and transport phenomena – building on the legacy of Keith Beven's work.

REFERENCES

Ameli AA, Abedini MJ. 2016. Performance assessment of low-order versus high-order numerical schemes in the numerical simulation of aquifer flow. *Hydrology Research* DOI:10.2166/nh.2016.148.

Ameli AA, Craig JR. 2014. Semianalytical series solutions for three-dimensional groundwater-surface water interaction. *Water Resources Research* **50**(5): 3893–3906.

Ameli AA, Craig JR, McDonnell JJ. 2015. Are all runoff processes the same? Numerical experiments comparing a Darcy-Richards solver to an overland flow-based approach for subsurface storm runoff simulation. *Water Resources Research* **51**(12) 10008–10028.

Ameli AA, Craig JR, Wong S. 2013. Series solutions for saturated–unsaturated flow in multi-layer unconfined aquifers. *Advances in Water Resources* **60**: 24–33.

Anderson M, Burt T. 1978. The role of topography in controlling throughflow generation. *Earth Surface Processes* **3**: 331–344.

Bakker M. 2013. Semi-analytic modeling of transient multi-layer flow with TTim. *Hydrogeology Journal* **21**: 935–943. DOI:10.1007/s10040-013-0975-2.

Bakker M, Nieber JL. 2004. Two-dimensional steady unsaturated flow through embedded elliptical layers. *Water Resources Research* **40**. DOI:10.1029/2004wr003295.

Beven K. 1983. Introducing spatial variability into TOPMODEL: theory and preliminary results. Report to Department of Environmental Sciences, University of Virginia.

Beven K. 1984. Infiltration into a class of vertically non-uniform soils. *Hydrological Sciences Journal* **29**: 425–434.

Beven K, Germann P. 2013. Macropores and water flow in soils revisited. *Water Resources Research* **49**: 3071–3092.

Beven K, Hornberger G, Germann P. 1989. Hillslope hydrology, a multiple interacting pathways model. In: Proceedings of the British Hydrological Society Second National Hydrology Symposium, Wallingford, UK, pp: 1-1.

Beven K, Kirkby M. 1979. A physically based, variable contributing area model of basin hydrology/Un modèle à base physique de zone d'appel variable de l'hydrologie du bassin versant. *Hydrological Sciences Journal* **24**: 43–69.

Birkel C, Tetzlaff D, Dunn SM, Soulsby C. 2011. Using lumped conceptual rainfall–runoff models to simulate daily isotope variability with fractionation in a nested mesoscale catchment. *Advances in Water Resources* **34**: 383–394.

Bishop K, Seibert J, Köhler S, Laudon H. 2004. Resolving the double paradox of rapidly mobilized old water with highly variable responses in runoff chemistry. *Hydrological Processes* **18**: 185–189.

Bishop K, Seibert J, Nyberg L, Rodhe A. 2011. Water storage in a till catchment. II: implications of transmissivity feedback for flow paths and turnover times. *Hydrological Processes* **25**: 3950–3959.

Botter G. 2012. Catchment mixing processes and travel time distributions. *Water Resources Research* **48**:(5). DOI:10.1029/2011WR011160.

Botter G, Bertuzzo E, Rinaldo A. 2010. Transport in the hydrologic response: Travel time distributions, soil moisture dynamics, and the old water paradox. *Water Resources Research* **46**:(3). DOI:10.1029/2009WR008371.

Botter G, Bertuzzo E, Rinaldo A. 2011. Catchment residence and travel time distributions: the master equation. *Geophysical Research Letters* **38**: (11). DOI:10.1029/2011GL047666.

Cardenas MB, Jiang X-W. 2010. Groundwater flow, transport, and residence times through topography-driven basins with exponentially decreasing permeability and porosity. *Water Resources Research* **46**n/a-n/a: . DOI:10.1029/2010wr009370.

Craig JR. 2008. Analytical solutions for 2D topography-driven flow in stratified and syncline aquifers. *Advances in Water Resources* **31**: 1066–1073. DOI:10.1016/j.advwatres.2008.04.011.

Cvetkovic V, Haggerty R. 2002. Transport with multiple-rate exchange in disordered media. *Physical Review E* **65**: 051308.

Davies J, Beven K, Rodhe A, Nyberg L, Bishop K. 2013. Integrated modeling of flow and residence times at the catchment scale with multiple interacting pathways. *Water Resources Research* **49**: 4738–4750.

Fiori A, Russo D. 2008. Travel time distribution in a hillslope: insight from numerical simulations. *Water Resources Research* **44**:(12). DOI:10.1029/2008WR007135.

Gardner W. 1958. Some steady-state solutions of the unsaturated moisture flow equation with application to evaporation from a water table. *Soil Science* **85**: 228–232.

Gisiger T. 2001. Scale invariance in biology: coincidence or footprint of a universal mechanism? *Biological Reviews of the Cambridge Philosophical Society* **76**: 161–209.

Godsey SE, Aas W, Clair TA, De Wit HA, Fernandez IJ, Kahl JS, Malcolm IA, Neal C, Neal M, Nelson SJ. 2010. Generality of fractal 1/f scaling in catchment tracer time series, and its implications for catchment travel time distributions. *Hydrological Processes* **24**: 1660–1671.

Grip H. 2015. Sweden's first forest hydrology field study 1905–1926: contemporary relevance of inherited conclusions and data from the Rokliden Hillslope. *Hydrological Processes* **29**(16): 3616–3631.

Haitjema HM, Mitchell-Bruker S. 2005. Are Water Tables a Subdued Replica of the Topography? *Ground Water* **0**050824075421008: . DOI:10.1111/j.1745-6584.2005.00090.x.

Harr RD. 1977. Water flux in soil and subsoil on a steep forested slope. *Journal of Hydrology* **33**: 37–58.

Heidbüchel I, Troch PA, Lyon SW. 2013. Separating physical and meteorological controls of variable transit times in zero-order catchments. *Water Resources Research* **49**: 7644–7657.

Hewlett JD, Troendle CA. 1975. Non point and diffused water sources: a variable source area problem. In: Watershed Management; Proceedings of a Symposium.

Hrachowitz M, Soulsby C, Tetzlaff D, Dawson J, Dunn S, Malcolm I. 2009. Using long-term data sets to understand transit times in contrasting headwater catchments. *Journal of Hydrology* **367**: 237–248.

Hrachowitz M, Soulsby C, Tetzlaff D, Malcolm I, Schoups G. 2010. Gamma distribution models for transit time estimation in catchments: physical interpretation of parameters and implications for time-variant transit time assessment. *Water Resources Research* **46**(10): DOI:10.1029/2010WR009148.

Jiang X-W, Wan L, Cardenas MB, Ge S, Wang X-S. 2010. Simultaneous rejuvenation and aging of groundwater in basins due to depth-decaying hydraulic conductivity and porosity. *Geophysical Research Letters* **37**n/a-n/a: . DOI:10.1029/2010gl042387.

Jiang X-W, Wan L, Wang X-S, Ge S, Liu J. 2009. Effect of exponential decay in hydraulic conductivity with depth on regional groundwater flow. *Geophysical Research Letters* **36**:. DOI:10.1029/2009gl041251.

Jiang XW, Wang XS, Wan L, Ge S. 2011. An analytical study on stagnation points in nested flow systems in basins with depth-decaying hydraulic conductivity. *Water Resources Research* **47**(1). DOI:10.1029/2010WR009346.

Kirchner JW, Feng X, Neal C. 2000. Fractal stream chemistry and its implications for contaminant transport in catchments. *Nature* **403**: 524–527.

Kirchner JW, Feng X, Neal C. 2001. Catchment-scale advection and dispersion as a mechanism for fractal scaling in stream tracer concentrations. *Journal of Hydrology* **254**: 82–101.

Klaus J, Chun KP, McGuire KJ, McDonnell JJ. 2015. Temporal dynamics of catchment transit times from stable isotope data. *Water Resources Research* **51**(6): 4208–4223.

Kollet SJ, Maxwell RM. 2008. Demonstrating fractal scaling of baseflow residence time distributions using a fully-coupled groundwater and land surface model. *Geophysical Research Letters* **35**(7). DOI:10.1029/2008GL033215.

Lundin L. 1982. Soil moisture and ground water in till soil and the significance of soil type for runoff.—UNGI Rapport Nr 56, Uppsala, 216 pp. Swedish, English summary.

Marklund L, Wörman A. 2007. The impact of hydraulic conductivity on topography driven groundwater flow. *Publications of the Institute of Geophysics Polish Academy of Sciences* **E-7**: 159–167.

Marklund L, Wörman A. 2011. The use of spectral analysis-based exact solutions to characterize topography-controlled groundwater flow. *Hydrogeology Journal* **19**: 1531–1543. DOI:10.1007/s10040-011-0768-4.

McDonnell JJ, Beven K. 2014. Debates—The future of hydrological sciences: a (common) path forward? A call to action aimed at

understanding velocities, celerities and residence time distributions of the headwater hydrograph. *Water Resources Research* **50**: 5342–5350.

Nyberg L. 1995. Water flow path interactions with soil hydraulic properties in till soil at Gårdsjön, Sweden. *Journal of Hydrology* **170**: 255–275.

Philip JR. 1957. The theory of infiltration: 4. Sorptivity and algebraic infiltration equations. *Soil Science* **84**: 257–264.

Pinay G, Peiffer S, De Dreuzy J-R, Krause S, Hannah DM, Fleckenstein JH, Sebilo M, Bishop K, Hubert-Moy L. 2015. Upscaling nitrogen removal capacity from local hotspots to low stream orders' drainage basins. *Ecosystems* **18**(6): 1101–1120.

Rinaldo A, Beven KJ, Bertuzzo E, Nicotina L, Davies J, Fiori A, Russo D, Botter G. 2011. Catchment travel time distributions and water flow in soils. *Water Resources Research* **47**(7). DOI:10.1029/2011WR010478.

Rodhe A. 1989. On the generation of stream runoff in till soils. *Nordic Hydrology* **20**: 1–8.

Salamon P, Fernàndez-Garcia D, Gómez-Hernández JJ. 2006. A review and numerical assessment of the random walk particle tracking method. *Journal of Contaminant Hydrology* **87**: 277–305.

Sayama T, McDonnell JJ. 2009. A new time-space accounting scheme to predict stream water residence time and hydrograph source components at the watershed scale. *Water Resources Research* **45**(7). DOI:10.1029/2008WR007549.

Seibert J. 1999. *On TOPMODEL's ability to simulate groundwater dynamics*. IAHS Publication(International Association of Hydrological Sciences); **254**: 211–220.

Seibert J, Bishop K, Nyberg L, Rodhe A. 2011. Water storage in a till catchment. I: distributed modelling and relationship to runoff. *Hydrological Processes* **25**: 3937–3949.

Seibert J, Bishop K, Rodhe A, McDonnell JJ. 2003a. Groundwater dynamics along a hillslope: a test of the steady state hypothesis. *Water Resources Research* **39**n/a-n/a: . DOI:10.1029/2002wr001404.

Seibert J, Rodhe A, Bishop K. 2003b. Simulating interactions between saturated and unsaturated storage in a conceptual runoff model. *Hydrological Processes* **17**: 379–390. DOI:10.1002/hyp.1130.

Srivastava R, Yeh TCJ. 1991. Analytical solutions for one-dimensional, transient infiltration toward the water table in homogeneous and layered soils. *Water Resources Research* **27**: 753–762.

Starn JJ, Bagtzoglou AC, Robbins GA. 2012. Methods for simulating solute breakthrough curves in pumping groundwater wells. *Computers & Geosciences* **48**: 244–255.

Toth J. 1963. A theoretical analysis of groundwater flow in small drainage basins. *Journal of Geophysical Research* **68**: 4795–4812.

Vaché KB, McDonnell JJ. 2006. A process-based rejectionist framework for evaluating catchment runoff model structure. *Water Resources Research* **42**(2). DOI:10.1029/2005WR004247.

Wang XS, Jiang XW, Wan L, Ge S, Li H. 2011. A new analytical solution of topography-driven flow in a drainage basin with depth-dependent anisotropy of permeability. *Water Resources Research* **47**(9). DOI:10.1029/2011WR010507.

Warrick A, Knight J. 2003. Steady infiltration from line sources into a layered profile. *Water Resources Research* **39**(12). DOI:10.1029/2003WR001982.

Warrick AW, Hinnell AC, Ferré TPA, Knight JH. 2008. Steady state lateral water flow through unsaturated soil layers. *Water Resources Research* **44**. DOI:10.1029/2007wr006784.

Weiler M, McGlynn BL, McGuire KJ, McDonnell JJ. 2003. How does rainfall become runoff? A combined tracer and runoff transfer function approach. *Water Resources Research* **39**(11). DOI:10.1029/2003WR002331.

Weyman D. 1973. Measurements of the downslope flow of water in a soil. *Journal of Hydrology* **20**: 267–288.

Zlotnik VA, Cardenas MB, Toundykov D. 2011. Effects of multiscale anisotropy on basin and hyporheic groundwater flow. *Groundwater* **49**: 576–583.